Available online at www.sciencedirect.com
ScienceDirect
International Journal of Heat and Mass Transfer 50 (2007) 1616–1630
International Journal of HEAT and MASS TRANSFER
www.elsevier.com/locate/ijhmt

Measurement of the dimensionless extinction coefficient of soot within laminar diffusion flames

T.C. Williams [a,*], C.R. Shaddix [a], K.A. Jensen [b,1], J.M. Suo-Anttila [b]

[a] Combustion Research Facility, Sandia National Laboratories, MS 9052, 7011 East Avenue, Livermore, CA 94551, United States
[b] Fire Science and Technology Department, Sandia National Laboratories, Albuquerque, NM 87185, United States

Received 16 February 2006; received in revised form 23 August 2006
Available online 25 October 2006

Abstract

The dimensionless extinction coefficient (K_e) of soot must be known to quantify laser extinction measurements of soot concentration and to predict optical attenuation through smoke clouds. Previous investigations have measured K_e for post-flame soot emitted from laminar and turbulent diffusion flames and smoking laminar premixed flames. This paper presents the first measurements of soot K_e from within laminar diffusion flames, using a small extractive probe to withdraw the soot from the flame. To measure K_e, two laser sources (635 nm and 1310 nm) were coupled to a transmission cell, followed by gravimetric sampling. Coannular diffusion flames of methane, ethylene and nitrogen-diluted kerosene burning in air were studied, together with slot flames of methane and ethylene. K_e was measured at the radial location of maximum soot volume fraction at several heights for each flame. Results for K_e at both 635 nm and 1310 nm for ethylene and kerosene coannular flames were in the range of 9–10, consistent with the results from previous studies of post-flame soot. The ethylene slot flame and the methane flames have lower K_e values, in some cases as low as 2.0. These lower values of K_e are found to result from the contributions of (a) the condensation of PAH species during the sampling of soot, (b) the wavelength-dependent absorptivity of soot precursor particles, and, in the case of methane, (c) the negligible contribution of soot scattering to the extinction coefficient. RDG calculations of soot scattering, in combination with the measured K_e values, imply that the soot refractive index is in the vicinity of 1.75–1.03i at 635 nm.

Keywords: Soot; Optical properties; Extinction coefficient; Diffusion flame; Scattering; PAH

1. Introduction

Accurate knowledge of the optical properties of soot particles is necessary for the proper interpretation of laser-based diagnostic measurements, for predicting radiant emission from sooty flames, and for predicting radiant extinction through smoke. One optical parameter of particular interest is the dimensionless extinction coefficient (K_e), which can be used to interpret laser extinction measurements of soot concentration via Bouguer's Law:

$$\frac{I}{I_0} = \exp\left(\frac{-K_e f_v}{\lambda} l\right) \tag{1}$$

where I/I_0 is the ratio of transmitted to incident monochromatic light intensity, f_v is the soot volume fraction, λ is the wavelength of light, and l is the path length through the medium. When combined with the scattering albedo (i.e. the ratio of scattering to extinction), K_e yields the dimensionless absorption coefficient, which is used in two-color pyrometry and for calculation of the thermal emission from hot soot.

In the last decade, a number of investigations have been conducted into the determination of the dimensionless extinction coefficient of soot, following the revelation by Choi and coworkers [1] that this quantity could not be accurately predicted from the Rayleigh limit expression

* Corresponding author. Tel.: +1 925 294 2396; fax: +1 925 294 2276.
E-mail address: tcwilli@sandia.gov (T.C. Williams).
[1] Present address: Pixia Corporation, R&D Staff, 45615 Willow Pond Plaza, Sterling, VA 20164, United States.

0017-9310/$ - see front matter © 2006 Elsevier Ltd. All rights reserved.
doi:10.1016/j.ijheatmasstransfer.2006.08.024

for K_e in combination with any of the standard literature values for the soot refractive index. The measurement of K_e typically involves simultaneous gravimetric sampling and light extinction (GSLE) measurements [1]. The GSLE approach has been used to establish K_e of soot emitted from laminar and turbulent diffusion flames and smoking laminar premixed flames for several fuels and over a range of visible and infrared wavelengths [1–10]. For all but underventilated diffusion flames [10], where difficulties arise from condensation of polycyclic aromatic hydrocarbons (PAH), K_e has been consistently measured to be between 8 and 10 in the wavelength range of 400 nm to 3 μm.

The GSLE systems used in these previous studies have collected soot via a hood above the flame or by enclosing the flame within a tube. These approaches simplify the collection of enough soot mass to make an accurate determination of soot sample weight. However, they are limited to sampling post-flame soot that has been emitted from the flame. In many cases laser extinction measurements are used to quantify the soot concentrations within diffusion flames, so it is important to establish the appropriate K_e value to use in interpreting these measurements. In addition, there are several reasons to believe that in-flame soot may have different optical properties than post-flame soot and that K_e may vary within the flame itself. One concern is to extent to which soot residence time in the flame affects the scattering component of extinction. In the soot inception region of flames, precursor particles are heated, undergo dehydrogenation and solidify into carbonaceous primary particles. As these particles are convected downstream they agglomerate to form progressively larger soot aggregates [11]. By the time these aggregates are sampled as post-flame soot, they have grown from individual primary particles to aggregates containing several hundreds of primaries [6]. Measurements have shown that light scattering from these large aggregates can account for between 20–30% of the total extinction [2,12,13]. In comparison the extinction of light by individual primary particles, low down in the flame, occurs almost entirely by absorption. Soot residence time therefore has the potential to significantly alter K_e. In a similar manner, different fuels, with different sooting propensities, may also affect K_e through changes in primary particle and aggregate size and therefore scattering albedo. Also, the extent to which thermal annealing of the soot within the flame or in the post-flame zone may increase its optical absorptivity (and therefore K_e) has not been definitively determined [14].

The current investigation is motivated by the desire to measure K_e of in-flame soot and to understand the effects that residence time and fuel type have upon it. Measurements of K_e are reported over a range of axial locations, and therefore, residence times, in methane/air, ethylene/air, and kerosene/nitrogen/air laminar diffusion flames. Investigation of these latter two flame systems allows comparisons to be made to post-flame K_e values available in the literature [7,9], as well as recent measurements of K_e from soot sampled within a JP-8 pool fire [15]. Following the work of previous sooting diffusion flame studies, K_e measurements were also conducted with the laminar flames operating in a 'pulsed' or 'flickering' mode [16–18].

To aid in the interpretation of the K_e measurements, the scattering component of K_e was estimated by applying Rayleigh–Debye–Gans theory of scattering and absorption by polydisperse fractal aggregates (RDG-PFA theory) to soot samples thermophoretically extracted from the flames and analyzed by transmission electron microscopy (TEM). Additional information was provided by performing a methylene chloride extraction of the bulk soot samples and comparing the ratios of organic to elemental carbon.

2. Experimental

2.1. Flame systems

Five different flames were interrogated in this study. All the flames were laminar, overventilated, normal jet diffusion flames, with fuel in the center surrounded by an abundant air coflow. Coannular flames of methane/air, ethylene/air and vaporized kerosene/nitrogen/air were investigated, as well as slot flames of methane/air and ethylene/air. Fuel and air flow parameters for the investigated flames are shown in Table 1.

Coannular and slot flame geometries were included in this study to determine their potential effect on K_e. The salient difference between the geometries lies in the heating of the central core of the flame, where soot formation occurs. In slot flames, the fuel stream is heated through planar diffusion, in contrast to cylindrical diffusion for coannular flames. This results in substantially faster heating of the fuel stream (as a function of height) for the coannular

Table 1
Flow conditions for the laminar diffusion flames

Flame	Q_{fuel} (slpm)	Q_{air} (slpm)	V_{fuel} (mm/s)	V_{air} (mm/s)	h_f (mm)[a]
C_2H_4 slot	7.5	250	112	176	~700
CH_4 slot	15.0	250	223	176	~700
C_2H_4 coannular	0.22	350	41	353	88
CH_4 coannular	0.44	350	82	353	84
Kerosene coannular	0.0335	350	26	353	40[b]
$+N_2$ diluent	0.107				

[a] Visible flame height.
[b] Height of strongly luminous zone (smoking flame without a well-defined flame height).

flames. For example, Roper's correlations for buoyant diffusion flame heights [19], computed on the basis of the diffusion rate of oxygen toward the fuel core, yield predicted flame heights of methane flames that are 2.5 times greater for slot flames, for equivalent fuel exit velocities and for the slot length used in this investigation. Soot would therefore be expected to form earlier and mature more rapidly in a coannular flame when compared to a similarly fueled slot flame. Indeed, at a height of 30 mm in the ethylene slot flame investigated here the peak soot volume fraction is approximately 2 ppm [20], whereas the peak soot volume fraction at this height in the coannular flame is approximately 9 ppm [17].

Two coannular burners were utilized, one to support the gaseous fueled methane/air or ethylene/air flames, the other to vaporize and support the kerosene flame. The burners had identical fuel tube and air coflow geometries so that direct comparisons could be made between the flames. A fuel tube diameter of 12.7 mm (1/2 in.) was selected to match that of previous workers [21–24]. In contrast to previous coannular flame studies, a square burner face (129 × 129 mm) and chimney enclosure was designed so that large, flat windows could be easily installed in the chimney walls for ease of performing planar laser/optical measurements.

The fuel flowrate in the ethylene flame was chosen to match the 88 mm visible flame height of the "non-smoking" flame extensively investigated in previous studies (e.g. [21,24]). The methane flowrate was chosen to yield a similar visible flame height (84 mm). For the liquid-fueled coannular burner, standard kerosene (obtained from a local hardware store) was gravity fed into a ceramic, capillary force vaporization system, which jetted vaporized fuel directly into the base of the electrically heated (350–380 °C) fuel tube. For stable operation of the flame, it was found that a small flow of nitrogen through the fuel tube was required to entrain and carry the heavy fuel vapor out of the tube. With kerosene vaporized at a rate of 12.5 g/h (equivalent to 0.0335 slpm), and 0.107 slpm nitrogen supplied to the base of the burner tube, a very stable and repeatable flame was achieved. The resulting smoking flame did not have a well-defined flame height but the strongly luminous zone extended to a height of 40 mm.

The air coflow for both coannular burners was chosen to give optimal stability in the steady flames and was set at 350 slpm, a flow that was considerably higher than that used in the "non-smoking" flame of previous work. In our burners, the flames were found to exhibit strong flickering at these lower airflow rates.

The slot flames were supported on a Wolfhard–Parker burner, the design of which has been reported previously [20]. Methane or ethylene was supplied to a central, 95 mm long and 12 mm wide, rectangular fuel slot. Air was supplied on each of the long sides of the fuel slot and a small flow of nitrogen gas, introduced at the fuel slot ends, was used to prevent the formation of 'end flames'. With curved wire mesh screens above the flame and a square chimney enclosure, the flame could be stabilized to give two near vertical flat flame sheets over the first ~100 mm of flame height. Total flame height, for either fuel, was approximately 700 mm.

For the pulsed flame measurements, the fuel flows were modulated upstream of the burner surface at a frequency of 15 Hz. In both gaseous-fueled coannular and slot burners, this modulation was achieved using loudspeakers. In the kerosene burner, the high temperature of burner tube prevented the use of a similar system. Instead a reciprocating model airplane piston, driven by an electric motor, was attached to a sidearm that connected into the vertical fuel tube.

2.2. Gravimetric sampling and light extinction (GSLE)

The dimensionless extinction coefficient of soot was measured using the portable GSLE apparatus originally used by Jensen and coworkers to make K_e measurements in large pool fires [15]. The apparatus (see Fig. 1) draws a sample stream through a probe, dilutes the sample with nitrogen, pulls it through a 1-m long transmission cell to allow accurate extinction measurements to be performed, and then passes a portion of the flow through a filter for determination of the entrained soot mass.

The sampling probe used by Jensen and coworkers was redesigned to allow sampling from the small diffusion flames under investigation here. Initially a tapered quartz

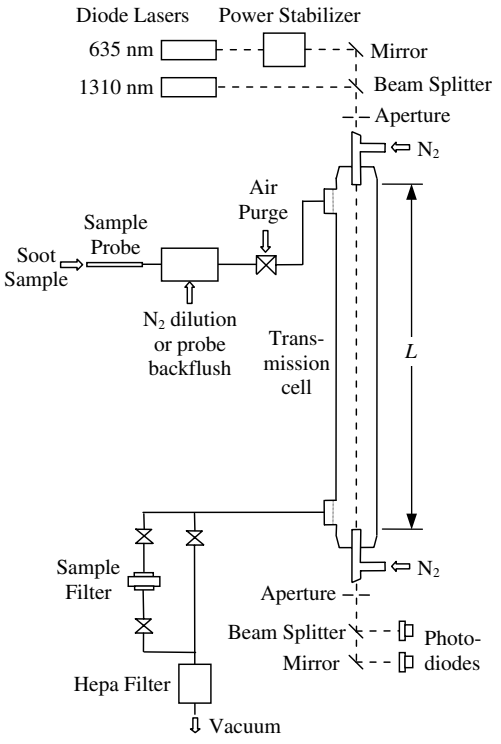

Fig. 1. Schematic of gravimetric sampling and light extinction (GSLE) apparatus.

microprobe was designed and constructed, based on a previous design [25,26]. The key operational feature of this probe was a solenoid-driven wire that protrudes through the tip of the probe to prevent tip blockage by soot. In practice, it was found that excessive buildup of soot and tar occurred within the probe, on the solenoid activated wire, and on the outside of the probe, when sampling from the kerosene flame and from either of the ethylene flames. These deposits resulted in a strongly time-dependent soot sampling efficiency and severe perturbation of the flame flowfield. To address these problems, a straight-cut stainless steel tube with a 3.2 mm outside diameter allowed sampling in the sootier flames without excessive buildup on the exterior of the probe. Further, by restricting the sample flow rate to 0.1 slpm, the probe had no noticeable effect on the local flame structure (though downstream perturbations in the flame were evident – see Fig. 2). Soot buildup did occur inside the tube when sampling regions with high soot density, but it was found that this flow restriction could be conveniently removed with a rapid backflush of nitrogen (5 slpm) out the end of the probe. When sampling from the ethylene and kerosene flames, up to two backflushes were needed during each ~10 min measurement period. For the methane flames no backflushes were required, but the low soot density then necessitated longer sampling periods of ~30 min.

From the entrance of the probe the sample traveled about 0.3 m before being diluted with 5 slpm of nitrogen (50:1 dilution ratio). The dilution served to quench any reactions and minimize soot agglomeration within the GSLE system. A further 2 m of tubing brought the sample to a wire mesh mixer and into the 1-m long transmission cell where the light extinction measurements were performed. Light extinction was performed simultaneously at 635 nm and 1310 nm with diode lasers whose beams were combined using a beam splitter and directed down the center of the transmission cell. After passing through the cell, the two beams were separated by a second beam splitter and directed onto two solid-state photodiode detectors. An aperture placed directly after the transmission cell reduced the acceptance angle of the photodiodes to ~1.5°, thus reducing contributions from forward scattering. The entrance and exit of windows of the transmission cell were canted to prevent back reflections onto the diodes and were purged with nitrogen to prevent soot deposition. Purge flowrates of nitrogen to the entrance and exit windows were 0.27 and 1.37 slpm, respectively.

Fig. 2. Photograph of stainless steel sample probe, extracting soot from the steady ethylene slot flame.

A portion of the flow exiting the transmission cell (~60%) was delivered through a Teflon filter so that the soot mass could be collected. The filter (with a weight of ~260 mg) was weighed before and after the sample period to determine the soot mass, using a Mettler scale with a resolution of 0.01 mg. Collected soot masses varied from 0.4 mg to 4.3 mg. To verify the absence of any moisture condensation on the soot, several filters representing high and low derived K_e values were re-weighed after being placed in a dessicator for several days and showed no change of mass.

GSLE measurements were made at heights of 25 mm, 45 mm, and 65 mm in the steady methane and ethylene slot and coannular flames. In addition, a measurement was made at a height of 10 mm in the steady ethylene slot flame. For the kerosene flame, with its shorter flame height, measurements were made at heights of 25 mm, 35 mm, and 45 mm. For the 15 Hz pulsed flames, all measurements were made at a height of 45 mm.

For the steady coannular flames the sample probe was positioned radially to the flame surface and held in the peak annular soot region, thus maximizing the amount of soot being sampled. For the pulsed coannular flames the probe was inserted further so that soot from the centerline of the flame was sampled. In the slot flames a similar procedure was followed, except in these flames the flame sheet was avoided by inserting the probe into the flame (~30 mm) from one of its open ends.

At most sampling locations, at least two measurements were performed to assess the reproducibility of the measurement. The spatial resolution of the sampling technique was deemed to be insufficient to effectively perform radial profiling through the thin soot layers. To optimize the consistency of the measurement in the different flames, the flowrates in the GSLE system were held constant throughout the series of measurements. Laminar flow elements were used to verify the indicated readings on the previously calibrated mass flow controllers.

2.3. Determination of K_e

The phenomena of soot probe clogging and nitrogen backflushing added a significant dynamic component to the laser attenuation signals collected, as shown in Fig. 3. Traditionally, K_e has been calculated by collecting soot mass during a period of steady laser attenuation and applying a rearranged form of Eq. (1), using average values of the laser attenuation and the total collected soot mass

$$K_e = \frac{-\lambda \ln(I/I_0)}{f_v l} = \frac{-\lambda \rho_{soot} V \ln(\bar{I}/I_0)}{m_{soot} l} \quad (2)$$

where ρ_{soot} is the density of soot, V is the volume of gas drawn into the transmission tube over the sample period, and m_{soot} is the total mass of soot pulled through the transmission tube. For application to situations where the instantaneous light extinction (and soot mass being collected) is varying significantly with time, Eq. (2) is only valid each instant in time (i.e., for each recorded data point) and must be integrated over the entire time period in which soot mass is being collected. This is equivalent to applying Eq. (2) using the total soot mass and the mean of $\ln(I/I_0)$ such that:

$$K_e = \frac{-\rho_{soot} V \frac{1}{T} \sum_{t=0}^{T} \ln(I_t/I_0)}{m_{soot} l} \quad (3)$$

where T is the length of the sample period in number of 'data points' and I_t is the transmission intensity at data point t. It should be noted that the volume flow of gas used in Eq. (2) and (3) includes the window purge flow introduced at the top of the transmission cell, in addition to the main flow of soot containing gases entering the transmission cell. In addition, since only a portion of the total flow exiting the transmission tube was directed through the Teflon filter, m_{soot} in Eq. (2) and (3) has to be calculated from the soot mass collected on the filter

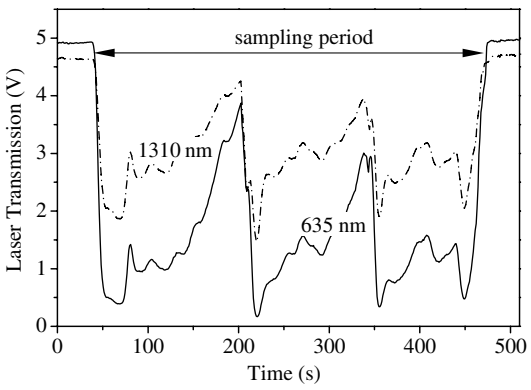

Fig. 3. Time record of laser transmission signals from the transmission cell when sampling from the steady ethylene slot flame at a height of 65 mm. The two rapid drops in transmission in the sampling period follow probe backflushing events, temporarily improving the sampling of soot from the flame.

$$m_{soot} = m_{collected\_soot} \cdot \frac{\dot{V}_{total}}{\dot{V}_{filter}} \quad (4)$$

where $\dot{V}_{filter}$ is the flow rate of sample directed through the filter and $m_{collected\_soot}$ is the mass of soot collected on the filter.

Using this analysis technique, K_e could be accurately determined even for sampling conditions in which several nitrogen backflushes were necessary during the sample period to prevent the probe from clogging.

The calculation of K_e requires knowledge of the density of soot. This quantity was not measured during this study and is a source of uncertainty in all K_e calculations, but is of particular concern here since the density of the collected "soot" is likely to show some variations from the contributions of tar-like material that is sampled together with the soot in the flame interior. This tar-like material may condense onto the soot or form a discrete aerosol as it cools in the sampling probe. The density of tar species generally falls between 1.0 and 1.2 g/cm^3, in comparison to a pure soot density of ~1.9 g/cm^3. For ease of interpretation and consistency with much of the K_e literature, the soot density is assumed here to be equal to 1.74 g/cm^3, as determined by Choi and coworkers [1] using helium pycnometry on post-flame soot from a premixed acetylene/air flame.

2.4. Methylene chloride extraction

In view of the concerns over the contribution of condensed hydrocarbons ("tar-like material") to the collected soot mass, vacuum extractions were performed on the collected soot mass using methylene chloride as the solvent. Approximately 20 ml of methylene chloride was pulled through each soot-containing filter, such that subsequent extractions showed no evidence of additional mass loss. The filters were then allowed to dry and were reweighed, to determine the mass of material that went into solution in the methylene chloride, herein defined to be the organic carbon content of the sample.

2.5. Soot microstructure and scattering albedo

Soot particles were collected onto TEM grids using a rapid insertion, short-hold, thermophoretic sampling technique [27] and were analyzed using a JEOL JEM 1200EX transmission electron microscope. Primary soot particle diameters and radius of gyration of the aggregates were then determined, and the scattering albedo estimated using the Rayleigh–Debye–Gans theory of scattering and absorption by polydisperse fractal aggregates (RDG–PFA theory) [28,29].

Soot samples were collected using carbon-coated TEM grids (200 mesh, 3 mm diameter), with the grids oriented vertically in an ultraslim grid holder, to minimize flame disturbance. The grid holder was mounted onto the end of a pneumatically driven piston with a 33 mm stroke length. Characteristic insertion and retraction times of the grids

were 6 ms, with the hold times varied depending on the local soot loading within the flame. The TEM grid samples were collected in the flame in a similar way to the GSLE sampling probe, with grids held on the flame centerline for pulsed flames and at the location of peak annular soot for the steady flames. For the steady coannular flames, this collection method ensured a good sample since the TEM grids straddled the entire soot layer. However, for the coannular flames the loaded TEM grids were briefly exposed to the high-temperature oxidation layer as they were retracted through the flame sheet. Collection in the steady slot flames presented greater alignment problems since the TEM grids were inserted in line with the soot layer. For the pulsed flames the TEM grids were positioned on the flame centerlines and held for several complete flame pulsing cycles.

The scattering albedo, ω_a, of a soot aerosol may be found from [28,29]

$$\overline{\omega_a} = \frac{\overline{\rho_{sa}^A}}{1 + \overline{\rho_{sa}^A}} \tag{5}$$

where

$$\overline{\rho_{sa}^A} = \frac{\overline{N^2}}{\overline{N}} \omega_p \left(1 + \frac{4}{3D_f} k^2 \overline{R_g^2}\right)^{-D_f/2} \tag{6}$$

is the population-averaged scattering-to-absorption ratio and the albedo of a primary particle is given as

$$\omega_p = \rho_{sa}^p = \frac{2}{3} k^3 r_p^3 \frac{F(\tilde{m})}{E(\tilde{m})} \tag{7}$$

In these equations: N is the number of primary particles in an aggregate, D_f is the fractal dimension (assumed to be 1.79 [6]), $k = 2\pi/\lambda$, R_g is the radius of gyration of the aggregate, r_p is the radius of a primary particle, and $F(\tilde{m})$ and $E(\tilde{m})$ are functions of the refractive index of soot. These functions are related to the complex refractive index, $m = n - ik$, using the following relationships:

$$F(\tilde{m}) \equiv \left|\frac{\tilde{m}^2 - 1}{\tilde{m}^2 + 2}\right|^2 = \frac{(n^2 - k^2 - 1)^2 + 4n^2k^2}{(n^2 - k^2 + 2)^2 + 4n^2k^2} \tag{8}$$

$$E(\tilde{m}) \equiv -\mathrm{Im}\left(\frac{\tilde{m}^2 - 1}{\tilde{m}^2 + 2}\right) = \frac{6nk}{(n^2 - k^2 + 2)^2 + 4n^2k^2} \tag{9}$$

To simplify the determination of the requisite soot aggregate parameters for calculation of the scattering albedo, the digitized TEM images were analyzed using an edge-detection program to obtain a binarized projected image of ~100 aggregates. The characteristic primary particle size was determined by visually fitting a circle to the primary particles, as they were present either individually or as part of soot aggregates. A total of approximately 50 primary particles were analyzed at each sampling location.

The radius of gyration, R_g, calculated on a pixel-by-pixel basis using the following relation [30]:

$$R_g = \sqrt{\frac{1}{N_{pixel}} \sum_{i=1}^{N_{pixel}} (r_i - r_c)^2} \tag{10}$$

where $(r_i - r_c)$ is the distance between the ith pixel and the center of mass of the aggregate and N_{pixel} is the number of pixels forming the aggregate.

The number of primary soot particles, N, constituting each aggregate was estimated using the following empirical relation and the correlation coefficients recommended by Köylü et al. [31]:

$$N = 1.15 \left(\frac{A_a}{\pi r_p^2}\right)^{1.09} \tag{11}$$

where A_a is the projected area of the aggregate and r_p is the radius of a primary soot particle.

3. Results and discussion

3.1. Flame structures and general trends in K_e

Presented in Fig. 4 are the measured values of K_e at 635 nm and 1310 nm for the five test flames, with each data set displayed as a function of height above the burner surface. By plotting the data in this manner, the K_e results are effectively displayed as a function of soot residence time in the flame. Results from recent investigations of post-flame soot emitted from JP-8 and ethylene flames have been added to the relevant plots in Fig. 4 to allow comparison with literature values [7,9,15]. No K_e values for a methane flame are available for comparison. Overall, the K_e results in Fig. 4 vary considerably, from 2 to 10, with the kerosene and ethylene coannular flames producing the highest K_e values and the methane slot flame the lowest.

To aid in the interpretation of the K_e results, Fig. 5 shows a series of OH radical laser-induced fluorescence (LIF) images of the five flames, with soot laser-induced incandescence (LII), PAH LIF and fuel LIF signals also visible in some of the images (Ref. [20] gives details of the laser imaging measurement procedures). Indicated on the images are the lower measurement heights where soot samples were extracted and the height at which incandescence from soot is just detectable using a 1064 nm laser light source. In the images, the effect of fuel type on sooting propensity is clearly evident with the kerosene flame producing soot much earlier in the flame and in greater quantities than the methane coannular flame. A striking difference between the flames is seen in the PAH fluorescence signals. Only the slot flames have strong PAH fluorescence signals at flame heights coincident with the sample locations. Broadband fluorescence (from both PAH and fuel vapor) is visible at the exit of the fuel tube of the kerosene flame image, but is restricted to low heights. It is believed that the PAH fluorescence persists to higher heights in the slot flames because these flames have lower heating rates of the fuel-rich core, delaying

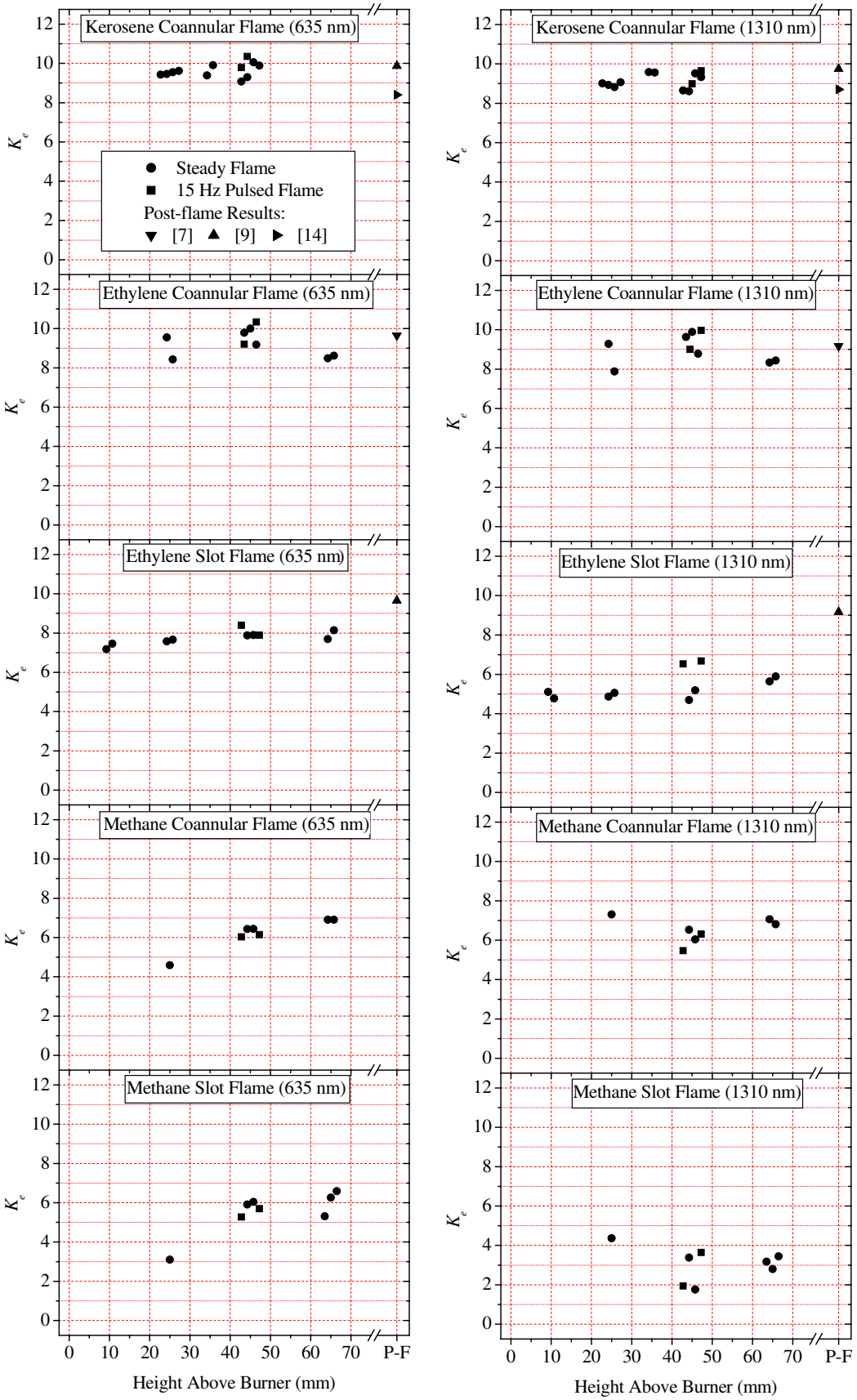

Fig. 4. Dimensionless extinction coefficients (K_e) of in-flame soot extracted from the five test diffusion flames over a range of flame heights. The left column of plots is the K_e data corresponding to a wavelength of 635 nm and the right column is the 1310 nm data. Repeat measurements at the same height are staggered slightly left–right so that they may be readily distinguished.

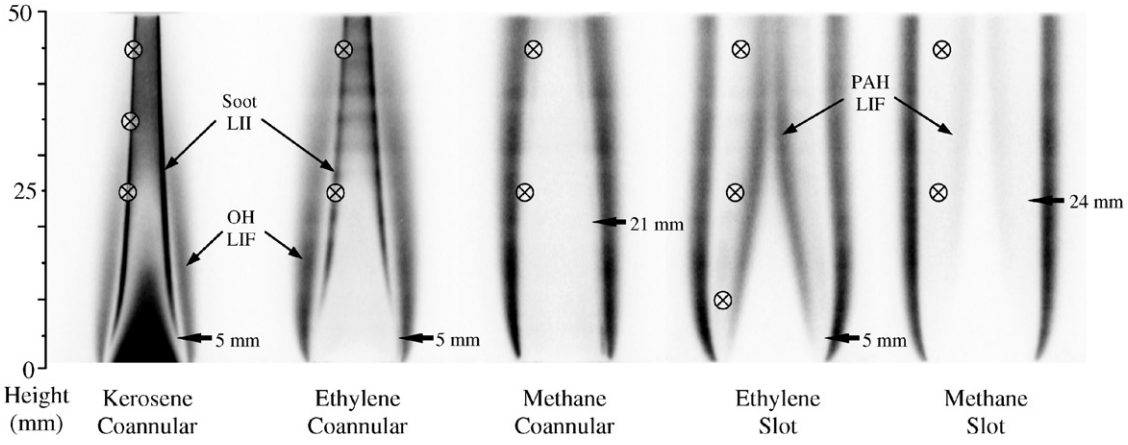

Fig. 5. Planar images of the test flames, showing OH· laser-induced fluorescence (Q_1 (8) line at 283.6 nm), PAH laser-induced fluorescence and laser-induced incandescence (LII) from soot. The circled crosses mark the flame heights where K_e soot samples were extracted. The horizontal arrows mark the heights at which soot LII, using a 1064 nm laser, was just detectable.

the conversion of PAH to soot. The heating rates are lower in the slot flames because of the planar geometry for thermal conduction of heat from the flamefront (as opposed to the cylindrical geometry present in coannular flames) and because of the nearly three-fold greater fuel exit velocity.

3.2. Kerosene and ethylene coannular flames

For the kerosene and ethylene coannular flames, the K_e results for both wavelengths fall into the 8 to 10 range (see Fig. 4), which is in good agreement with past work. Zhu and coworkers [9] measured post-flame soot emitted from a laminar JP-8 diffusion flame, yielding a K_e value of 9.9 at 632.8 nm and 9.8 at 1314 nm (JP-8 is the US military aviation fuel blend and is a form of kerosene). Measurements of soot extracted from the flame zone of a large JP-8 pool fire, where the soot sample is most likely a mixture of overfire and in-flame soot, yielded K_e values between 7 and 9 for both 635 nm and 1310 nm, with a slight trend towards higher values at 635 nm [15]. Measurements of the post-flame soot from an ethylene laminar diffusion flame yielded a K_e value of 9.7 at 632.8 nm and 9.2 at 1314 nm [7].

The K_e results for these two flames do not show any significant variation with flame height. However, the scatter present in the data (approximately 10% at some flame heights) masks any subtle trends with height that may exist. Comparing the results for the two wavelengths for these flames, K_e has a small bias to lower values at 1310 nm. The mean K_e value at 635 nm is 9.7 for the kerosene flame and 9.3 for the ethylene flame. These compare to 1310 nm mean values of 9.2 and 9.0 for the kerosene and ethylene flames, respectively.

For these coannular flames, the lack of significant variation of K_e, both within the flame (for the heights investigated) and between in-flame and post-flame soot, is an extremely convenient result, both for the interpretation of optical measurements of soot concentration and for predictions of radiant extinction through smoke or soot. Fig. 6 shows TEM images of typical soot aggregates extracted from the kerosene and ethylene flames at a height of 45 mm. Classic soot aggregates can be seen with spherical soot primaries fused together to form chain structures. The results of the RDG–PFA analysis of the soot aggregate fields are presented in Table 2, with scattering albedos calculated using several refractive indexes [6,32–35]. Results are presented for all five flames at a height of 45 mm and for the ethylene coannular flame over a range of flame heights. Only the soot particles extracted from the kerosene and ethylene coannular flames have notable scattering albedos. At a wavelength of 635 nm the albedo ranges from 17% to 30% for the kerosene coannular flame, depending on the assumed refractive index, and between 11% and 21% for the ethylene flame. The soot scattering albedo in the ethylene coannular flame is essentially constant from a height of 25 mm and upwards.

The small bias to lower K_e values at longer wavelengths has been seen in previous studies. When measuring post-flame soot from an ethylene diffusion flame, Zhu and coworkers [7] reported a slight reduction in K_e (~5%) as the wavelength was increased from 632.8 nm to 1314 nm. Measurements of post-flame soot from a JP-8 flame [15] showed, after an initial rise in K_e in the visible wavelengths, a similar decrease in K_e in the near-infrared. In both of these studies the wavelength dependence of K_e became less sensitive as the wavelength was extended further into the infrared, with little effect seen on K_e as the wavelength was increased from 1314 nm to 1565 nm. The dependence of K_e on wavelength in these studies was attributed to a diminishing contribution of scattering to the total extinction, although it was noted that there is considerable uncertainty in the spectral dependence of the refractive index of soot. In the present study, the RDG–PFA calculations for the ethylene and kerosene coannular soot show a substantial reduction in scattering albedo between 635 nm and 1310 nm, for most choices of refractive index at these two wavelengths (Table 2). For example, if the refractive index

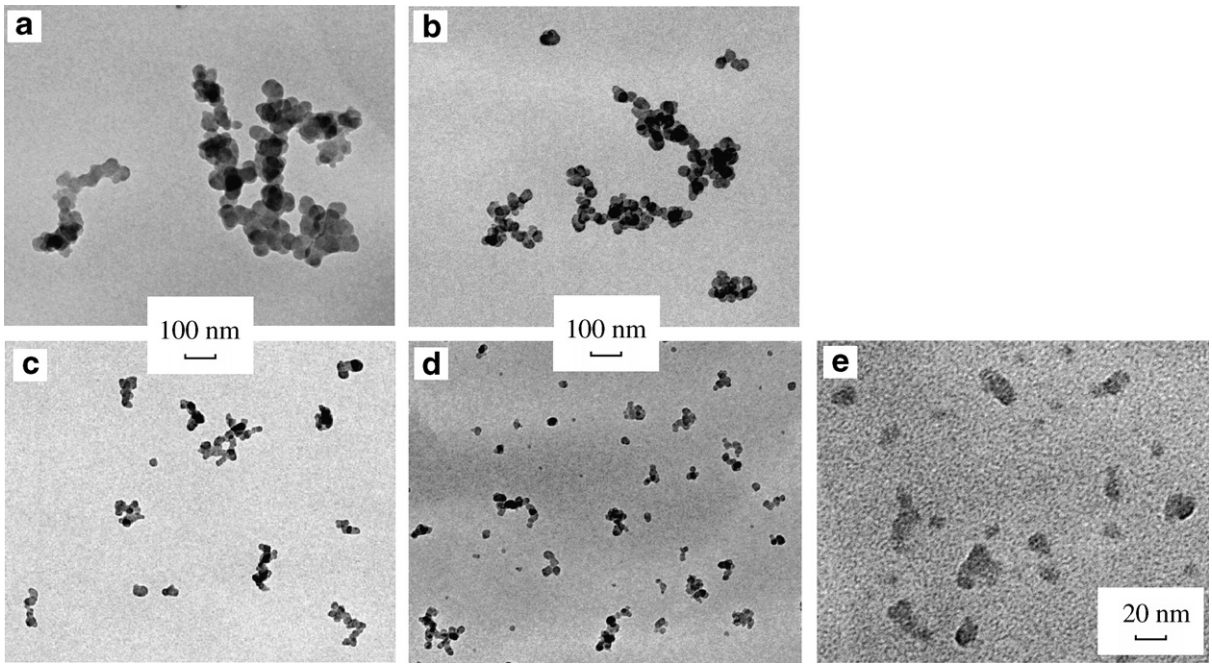

Fig. 6. TEM images of typical soot aggregates at a flame height of 45 mm from flames: (a) kerosene coannular, (b) ethylene coannular, (c) ethylene slot, (d) methane coannular and (e) methane slot. *Note*: Due to a missed TEM sample, image (c) corresponds to a flame height of 65 mm.

dispersion relation of Lee and Tien [34] is used, then the scattering albedo for the kerosene soot is predicted to decrease from 0.3 at 635 nm to 0.05 at 1310 nm, equating to a 26% reduction in K_e. This compares to a measured reduction in K_e of less than 5%. The reason for this difference is not fully understood, but it suggests a problem either with application of the RDG–PFA theory to the soot in these flames or with the reported values for the refractive index of soot. Zhu and coworkers [36] highlighted an inconsistency between RDG–PFA predictions and scattering albedo by measuring the scattering and extinction of post-flame ethylene soot with a transmission cell reciprocal nephelometer. Contrary to the expected diminishment in the scattering contribution at longer wavelengths, they observed an increase in scattering albedo as the wavelength increased from 632.8 nm into the near infrared.

In a study of post-flame soot from an acetylene diffusion flame, K_e was found to increase with wavelength [7]. This departure from the downward trend seen in K_e studies of ethylene and JP-8 flames was attributed to beam shielding effects [37,38], which are expected to become more significant with the large primary particles and more compact aggregation of acetylene soot. Beam shielding, which can substantially reduce the absorption cross section of soot particles, diminishes in significance as wavelength increases [37].

3.3. Ethylene slot flame

The K_e results for the ethylene slot flame (Fig. 4) show the same apparent invariance to flame height seen in the kerosene and ethylene coannular flames, but they also exhibit two striking differences. First, the K_e values are significantly lower (16–21%) than those of the corresponding coannular flame. At a measurement wavelength of 635 nm the mean K_e value of the ethylene slot flame is 7.8, compared to 9.3 for the ethylene coannular flame. Second, the K_e results show considerably more variation with wavelength. At 1310 nm the mean K_e value is 5.4, 31% lower than the value at 635 nm.

On first inspection, the lower K_e values seen in the ethylene slot flame could simply be a result of the presence of soot with a smaller scattering cross-section than is seen in the more rapid soot formation regimes of the ethylene and kerosene coannular flame geometries. The TEM images in Fig. 6 support this view, with the soot extracted from the ethylene slot flame exhibiting lower levels of aggregation and consisting of smaller primary particles. In the RDG–PFA prediction of scattering albedo (see Table 2), which is particularly effected by primary particle diameter, the scattering albedo in the slot flame at 635 nm is calculated to be ~4%, compared to ~20% for the ethylene coannular flame. This difference in scattering contribution conveniently accounts for the difference observed in the K_e results at 635 nm, but is unable to explain the large deviation in measured K_e values for the two flames in the near-infrared.

Fig. 5 suggests that the extractive sampling of soot from the slot flames is likely to include partial sampling of the adjacent PAH layer, potentially contaminating the gravimetric soot samples with condensed PAH. Indeed, the horizontal separation between the centers of the PAH and soot layers is 2–3 mm the slot flames, with an overlap of the layers at the edges. PAH with a molecular mass less than

Table 2
Soot structure properties and estimated scattering albedos for a range of refractive indices of soot

Flame (all steady)	Height (mm)	$d_p \pm 1\sigma$ (nm)	$\overline{N}$	$\overline{N^2}/\overline{N}^2$	R_g (nm)	$\overline{R_g^2}$ (nm^2)	Aggregate scattering albedo 635 nm			Aggregate scattering albedo 1310 nm		
							$m = 1.99–0.89i$[a]	$m = 1.90–0.43i$[b]	$m = 1.57–0.56i$[c]	$m = 2.33–0.78i$[d]	$m = 1.90–0.74i$[b]	$m = 1.72–0.80i$[e]
Kerosene coannular	45	41 ± 11	30	2.39	74	9460	0.29	0.30	0.17	0.09	0.05	0.04
C_2H_4 coannular	45	36 ± 6	26	2.12	62	5320	0.20	0.21	0.11	0.05	0.03	0.02
C_2H_4 slot	65[f]	25 ± 5	13	2.20	28	1090	0.05	0.05	0.02	0.01	0.01	0.00
CH_4 coannular	45	20 ± 4	8	3.64	18	492	0.03	0.03	0.02	0.01	0.00	0.00
CH_4 slot	45	11 ± 3	3	2.07	6	41	0.00	0.00	0.00	0.00	0.00	0.00
C_2H_4 coannular	65	25 ± 5	62	2.80	70	6480	0.21	0.22	0.12	0.06	0.03	0.03
C_2H_4 coannular	45	36 ± 6	26	2.12	62	5320	0.20	0.21	0.11	0.05	0.03	0.02
C_2H_4 coannular	25	45 ± 9	9	3.01	38	2240	0.22	0.23	0.13	0.05	0.03	0.02

[a] Krishnan et al. [6]. Deduced from RDG–PFA analysis of overfire soot from turbulent diffusion flames.
[b] Dispersion model of soot by Lee and Tien [34]. Predicted spectral refractive index at $\lambda = 635$ nm and $\lambda = 1310$ nm for at a soot temperature of 1000 K.
[c] Dalzell and Sarofim [32] and Smyth and Shaddix [33]. Refractive indices of acetylene and propane soot at visible wavelengths from reflectometry measurements of compressed soot pellets.
[d] Felske et al. [35]. Refractive indices of propane soot particles at $\lambda = 2.0$ μm from reflectometry measurements of compressed soot pellets.
[e] Dalzell and Sarofim [32] and Smyth and Shaddix [33]. Interpolated values corresponding to $\lambda = 1310$ nm using dispersion formula.
[f] Due to a missing TEM sample at 45 mm flame height, RDG–PFA results for the 65 mm flame height have been used instead.

~450 amu is transparent to light at visible and infrared wavelengths [39], so any increase in collected mass from condensed PAH collected on the GSLE filter will reduce the derived K_e. Examination of the methylene chloride-soluble mass fractions reveals that indeed significant organic content is present in the GSLE samples extracted from the two slot flames. The mean organic mass fractions across all sample heights are 32% and 25% for the methane and ethylene slot flames, respectively. In contrast, no measurable amount of mass was removed by the solvent from either the kerosene or ethylene coannular flame samples.

Fig. 7 shows the effect on K_e that contamination by condensed PAH would have, if it is assumed that the PAH is transparent to light at the wavelengths used in this study. In Fig. 7 the mass-adjusted values of K_e for the three flames, which contained organic carbon content in their soot samples, are displayed along with the original K_e values from Fig. 4. The ethylene slot flame results show a consistent increase in K_e when the organic mass is removed from the calculation. The mean adjusted K_e value at 635 nm increases to 9.9 from the uncorrected value of 7.8. At 1310 nm the mean adjusted K_e value is 6.9 compared to the previous value of 5.4. These corrections reduce the difference in K_e values seen between the ethylene slot and ethylene coannular flames, particularly at 635 nm.

Consideration of the combined effects of condensed PAH contamination and reduced scattering albedo on K_e still leads to inconsistencies in the ethylene slot flame in comparison to the coannular flame. At 635 nm, the mean PAH-adjusted K_e value for the ethylene slot flame is 9.9. When the effect of the reduced scattering albedo is also taken into consideration, this K_e value should be approximately 17% *lower* than the K_e value obtained for the ethylene coannular flame (9.3), not higher than this value. This inconsistency can be reconciled, however, by recognizing that at the heights sampled in the slot flame, it is likely that soot precursor particles, formed in the soot inception zone at the boundary between the PAH layer and the soot layer, are sampled together with mature carbonaceous soot. These precursor particles are known to have a lower mass density ($\rho = \sim 1.2$ g/cm^3) [40] in comparison to that of mature, carbonaceous soot ($\rho = \sim 1.74$ g/cm^3). This implies that the gravimetric soot samples collected from the slot flames have a lower soot mass density than has been used in the calculation of K_e in this study (direct measurements of soot density were not feasible). A lower soot density reduces the derived K_e in Eq. (2). To be consistent with the ethylene coannular K_e value and taking into consideration the organic mass fraction and difference in scattering albedo, the K_e value for the ethylene slot flame should equal ~7.8. The mean density of the soot extracted from the ethylene slot flame required to achieve this is 1.4 g/cm^3.

Further evidence of the contribution of soot precursor particles to the sample stream extracted from the ethylene slot flame is provided by the observation of a significant wavelength dependence in the K_e results for the ethylene (and methane) slot flame. As the earliest particles are

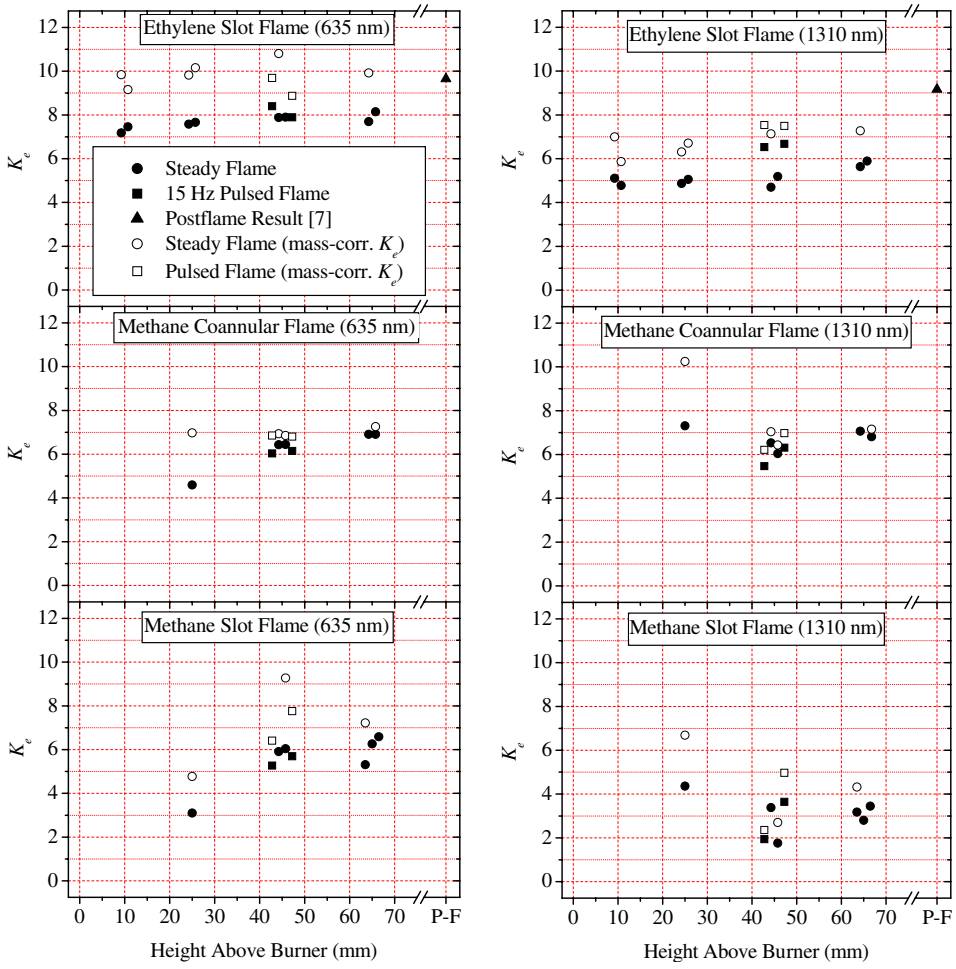

Fig. 7. Comparison of the mass-corrected (for organic content) K_e data with the uncorrected data contained in Fig. 4. The soot samples from the kerosene and ethylene coannular flame contained no significant organic content.

heated and carbonize in a flame to form mature soot, they transition from only absorbing light at ultra-violet (UV) wavelengths to absorbing light over a broader band that extends into the infrared [41]. The maturity of soot particles is typically characterized by the molar H/C ratio, with precursor particles having an H/C ratio of between approximately 0.25–0.6 and mature, carbonaceous soot an H/C ratio less than 0.2 [11,40,42]. On average, the soot samples from the slot flame contain less mature soot, with a higher H/C ratio, than soot at the same flame height in the coannular burner (producing the lower mean soot density, as discussed above). In an early work by Millikan [43], the optical extinction dispersion exponent of soot deposits was found to be a function of the molar H/C ratio. In terms of K_e, the measurements from 400 nm to 1000 nm showed that for mature soot, with an H/C ratio of 0.2, $K_e \propto 1/\lambda^{0.2}$, and for precursor particles, with an H/C ratio of 0.5–0.6, $K_e \propto 1/\lambda$. This gives an explanation, in terms of the chemical composition of the soot, for the K_e trends observed in both slot flames as a function of wavelength. More recently, the empirical relationship between absorption properties and H/C ratio has been reinterpreted by Minutolo and coworkers [41] in terms of the energy separation between valence and conduction electrons of aromatic clusters within incipient soot particles.

3.4. Methane flames

The K_e results for the methane coannular flame (Figs. 4 and 7) are substantially lower than the values obtained for kerosene and ethylene fueled coannular flames. The TEM images (Fig. 6) reveal small soot aggregates in the methane coannular flame with calculated scattering albedos less than 3% at 635 nm. Extinction of light by methane soot aggregates is therefore almost exclusively through absorption, producing a lower K_e value than seen with the larger soot aggregates of flames fueled with heavier hydrocarbons. The samples from the methane coannular flame contain organic carbon content, particularly at the lowest measurement height of 25 mm where the organic mass fraction is 34%. At sample heights above 25 mm, the organic mass fraction falls to less than 7%, which lends confidence to the K_e values at these locations. The apparently errant K_e values at 25 mm (for both methane flames) presumably

result from sampling close to the soot inception point, producing very low light attenuation in the transmission tube and necessitating soot collection over time periods of 20–30 min (yielding less than 1 mg of soot). Discounting these values, the mean mass-corrected K_e values are 6.9 at 635 nm and 6.8 at 1310 nm, less than 6% higher than the uncorrected values of 6.5 and 6.4. If one were to then include a scattering albedo of 25–30%, as typically measured for highly aggregated soot (as seen in the ethylene and kerosene coannular flames), the effective K_e would be in the 9.0–9.6 range.

The K_e results for the methane slot flame are difficult to interpret, with a large scatter of the mass-corrected K_e values, probably resulting from the low light attenuation, long sampling periods, and relatively small soot masses collected in this flame. At 635 nm the uncorrected K_e value of 6.0 is just slightly lower than the result for the methane coannular flame. However, the methylene chloride extraction shows ~20–35% condensed PAH in the gravimetric samples, yielding PAH-corrected K_e values in the range of 7 to 8. The TEM imaging shows very small soot particles, with little agglomeration and negligible scattering albedos. The particles are irregularly shaped and appear to have a liquid-like, translucent composition, typical of precursor particles seen elsewhere [11]. The molar H/C ratio would therefore be expected to be approximately 0.4 with a dispersion exponent of 1.6 [43] (giving $K_e \propto 1/\lambda^{0.6}$). This agrees with the observed ~40% reduction in (PAH-corrected) K_e to 4 to 5 as the wavelength is doubled from 635 nm to 1310 nm. As explained in discussing the ethylene slot flame, the sampling of precursor particles leads to an overestimation of the true K_e, because of the lower mass density of the collected soot. Therefore, the true K_e in the methane slot flame is somewhat lower than the PAH-corrected values.

3.5. Implications for soot refractive index

The methane coannular flame K_e measurements, with negligible calculated scattering contribution to extinction and negligible contribution of condensed PAH and soot precursor particles, imply that the dimensionless absorption coefficient (K_a) of soot in this flame is approximately 7.0 at both 635 nm and 1310 nm. If it is assumed that the optical absorptivity of carbonaceous soot particles is relatively independent of fuel source and flame type, as long believed and recently supported [14], then it follows that with $K_a = 7.0$, the soot scattering albedos for the ethylene and kerosene coannular flames are in the range of 20–30%. These results have substantial implications for the refractive index of soot, since they are not accurately predicted by index of refraction values reported in the literature, as interpreted with RDG theory. For instance, the proposed K_a value of 7.0 is substantially larger than the value of 4.9 that applies for Rayleigh-limit absorption of primary particles using the Dalzell and Sarofim [32] and Smyth and Shaddix [33] value of 1.57–0.56i for the soot refraction index. Use of the Lee and Tien [34] dispersion formula refractive index of 1.90–0.43i at 635 nm gives an even smaller Rayleigh-limit K_a of 2.9. Krishnan et al. [6] index of refraction of 1.99–0.89i yields the highest K_a value of the three, with a value of 5.1. Mountain and Mulholland [37] found that a soot refractive index of $m = 1.55–0.8i$ gave good predictions of K_e when using a discrete dipole method to calculate soot aggregate absorption and scattering. This value of the refractive index yields a Rayleigh-limit K_a of 6.9, which is in good agreement with the current work. However, it gives low RDG–PFA predictions of the scattering albedo of 0.1–0.2 at 635 nm for the soot particles in the kerosene and ethylene flames.

To generate K_a and scattering albedo values at 635 nm that are consistent with the current K_e measurements, relatively high values for both the real (n) and imaginary parts (k) of the refractive index are required. These solutions for n and k are represented graphically in Fig. 8. In the figure, both the Rayleigh-limit absorption of primary particles ($K_a = 6\pi E(m)$) and the scattering albedo (Eq. (5)) are solved in terms of 'n' and 'k', producing the ellipses seen. The intersection of these ellipses gives a solution for the refractive index. For the Rayleigh-limit absorption, an ellipse corresponding to a constant K_a of 7.0 is plotted, together with ellipses for $K_a = 6.5$ and $K_a = 7.5$. The ellipses of constant scattering albedo have been calculated using the primary particle diameter and aggregate structure properties of the soot collected from the ethylene coannular flame at a height of 45 mm (Table 2). A scattering albedo of 0.25 for the ethylene coannular flame, corresponding to $K_e = 9.3$, has been used, together with a lower value of 0.17. This lower value has been calculated using

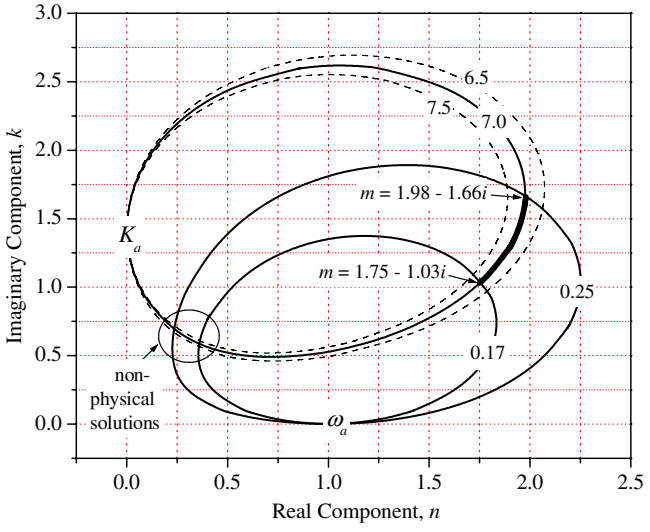

Fig. 8. Solutions of the real and imaginary components of the refractive index of soot at 635 nm that are consistent with particular values of the non-dimensional absorption coefficient, K_a, or the scattering albedo, ω_a, chosen per the description in the main text. The intersections of the ellipses denote index values that match both the assumed K_a and ω_a values and are consistent with the current K_e measurements. Values of the real part of the refractive index less than one are considered non-physical.

the lowest individual K_e measurement (8.4) taken in the ethylene coannular flame, and marks the lowest feasible scattering albedo for the assumed $K_a = 7.0$. This range of scattering albedos gives approximate bounds to the possible values for refractive index that are consistent with the current K_e measurements, defined by a curve from $m = 1.75–1.03i$ to $m = 1.98–1.66i$. The real component of the refractive index along this curve is consistent with a number of previous studies. The lower end of this curve gives an imaginary component of the index of refraction of ~1.0, which is just slightly greater than the value recently determined by Krishnan et al. [6]. The upper end of this curve gives an imaginary component of ~1.5, which is significantly larger than any value of 'k' previously suggested for soot. However, measurements for graphitic carbon often give values of 'k' of this magnitude [44].

Performing an equivalent analysis of the implications of the current measurements on the index of refraction at 1310 nm proves to be more difficult. Approaching the problem with the same assumption as used above for 635 nm (namely, $K_{a,ethylene} = K_{a,methane}$) yields a K_a of 7.0 and a scattering albedo of ~0.22 at 1310 nm for the ethylene coannular flame soot. As shown in Fig. 9, these values for K_a and the scattering albedo are incompatible at 1310 nm (i.e. they do not yield a rational solution for the refractive index). If we approach the problem from another angle, and assume that the RDG predictions (using literature values of the refractive index) of a scattering albedo of ~5% at 1310 nm are correct, then our measured K_e values imply a K_a for the ethylene coannular flame of 8.6. Using these values, the analysis shown in Fig. 9 yields a refractive index of 1.63–2.00*i*. A value of two for the imaginary component of the index is high in comparison to reported measurements of the soot refractive index in the infrared [32,34,35], which tend to cluster near a value of one for wavelengths in the vicinity of 1–2 micrometers, but some measurements of 'k' for graphitic materials in the infrared yield values of two [45].

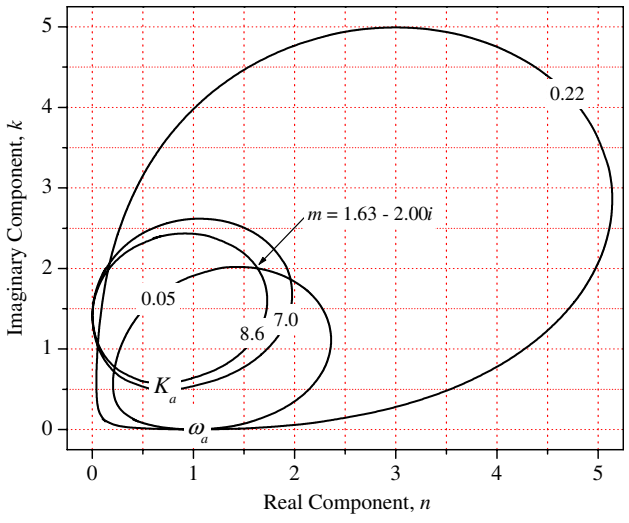

Fig. 9. Solutions of the real and imaginary components of the refractive index of soot at 1310 nm that are consistent with particular values of the non-dimensional absorption coefficient, K_a, or the scattering albedo, ω_a, chosen per the description in the main text. The intersections of the ellipses denote index values that match both the assumed K_a and ω_a values and are consistent with the current K_e measurements. Values of the real part of the refractive index less than one are considered non-physical.

Revisiting the analysis for the 635 nm data that was presented in Fig. 8, it is seen that relaxing the assumption that $K_{a,ethylene} = K_{a,methane}$ does not have a significant effect on the derived refractive index. This is because experimental measurements of the scattering albedos at 635 nm (typically between 0.15 and 0.35) have shown a reasonably good agreement with RDG-calculated values (using conventional indices of refraction) [7,13]. Therefore, as shown in Table 2, an assumption of a scattering albedo for the ethylene coannular flame soot of 0.15–0.20 appears reasonable, yielding a K_a of 7.5–8.0. The refractive index at 635 nm that is consistent with these requirements is close to the value of 1.75–1.03*i* previously derived.

4. Conclusions

After development of an effective, non-disruptive means of sampling soot from within a flame, the dimensionless extinction coefficient, K_e, was measured at several heights within both coannular and slot diffusion flames of methane, ethylene, and nitrogen-diluted kerosene burning in air. The coannular ethylene and kerosene flames consistently yielded K_e values of ~9.5 at 635 nm and ~9.0 at 1310 nm, with a trend towards slightly higher values in the kerosene flame. These values and trends are consistent with previous K_e measurements of post-flame soot derived from diffusion flames of these fuels. The ethylene slot flame K_e values are substantially lower than the ethylene coannular flame K_e, especially in the near-infrared, yielding average values of 7.8 at 635 nm and 5.4 at 1310 nm. Methylene chloride extraction of the collected soot shows that there is about 25% organic content in the slot flame soot, compared to negligible organic content in the coannular ethylene and kerosene flame soot. This finding, together with qualitative evidence provided by planar imaging of the PAH and soot fields in these flames, suggests that the lower apparent K_e value at 635 nm results from the contribution of optically transparent condensed PAH species that are captured on the gravimetric sampling filter together with the soot. TEM imaging and RDG analysis of soot samples collected from the flames also shows that the soot particles in the slot flames are smaller and less aggregated and therefore contribute less optical scattering towards the total optical extinction. The very low value of K_e in the near-infrared for the ethylene slot flame appears to result from sampling condensed PAH and soot precursor particles together with carbonaceous soot in the slot flames, at heights where soot inception is still active. The methane coannular flame produced K_e values of 6.5 at 635 nm and 6.4 at 1310 nm. There was a small (~6%)

contribution of organic carbon in the collected soot samples for this flame. Particle scattering calculations show a negligible scattering albedo for the methane flame in comparison to albedos of 0.2–0.3 in the ethylene and kerosene coannular flames, thereby accounting for the lower measured K_e values in the methane flame. The methane slot flame results show similar effects of PAH and soot precursor particle sampling as were evidenced in the ethylene slot flame. RDG calculations of soot scattering, in combination with the measured K_e values, imply that the soot refractive index is in the vicinity of $1.75–1.03i$ at 635 nm. At 1310 nm, the implied refractive index is somewhat different for methane and ethylene soot.

Acknowledgements

Funding for this work was provided by the Laboratory Directed Research and Development program of Sandia National Laboratories. Nancy Y.C. Yang of Sandia is gratefully acknowledged for her assistance in performing the TEM work. Sandia is a multi-program laboratory operated by Sandia Corporation, a Lockheed Martin Company, for the United States Department of Energy under contract DE-AC04-94-AL85000.

References

[1] M.Y. Choi, G.W. Mulholland, A. Hamins, T. Kashiwagi, Comparisons of the soot volume fraction using gravimetric and light extinction techniques, Combust. Flame 102 (1995) 161–169.
[2] J.S. Wu, S.S. Krishnan, G.M. Faeth, Refractive indices at visible wavelengths of soot emitted from buoyant turbulent diffusion flames, J. Heat Transfer 119 (1997) 230–237.
[3] G.W. Mulholland, M.Y. Choi, Measurement of the mass specific extinction coefficient for acetylene and ethene smoke using the large agglomerate optics facility, Proc. Combust. Inst. 27 (1998) 1515–1522.
[4] Z.Q. Zhou, T.U. Ahmed, M.Y. Choi, Measurement of dimensionless soot extinction constant using a gravimetric sampling technique, Exp. Thermal Fluid Sci. 18 (1998) 27–32.
[5] J. Zhu, M.Y. Choi, G.W. Mulholland, L.A. Gritzo, Measurement of soot optical properties in the near-infrared spectrum, Int. J. Heat Mass Transfer 43 (2000) 3299–3303.
[6] S.S. Krishnan, K.C. Lin, G.M. Faeth, Optical properties in the visible of overfire soot in large buoyant turbulent diffusion flames, J. Heat Transfer 122 (2000) 517–524.
[7] J. Zhu, M.Y. Choi, G.W. Mulholland, S.L. Manzello, L.A. Gritzo, J. Suo-Anttila, Measurement of visible and near-IR optical properties of soot produced from laminar flames, Proc. Combust. Inst. 29 (2002) 2367–2374.
[8] J.F. Widmann, J.C. Yang, T.J. Smith, S.L. Manzello, G.W. Mulholland, Measurement of the optical extinction coefficients of post-flame soot in the infrared, Combust. Flame 134 (2003) 119–129.
[9] J. Zhu, A. Irrera, M.Y. Choi, G.W. Mulholland, J. Suo-Anttila, L.A. Gritzo, Measurement of light extinction constant of JP-8 soot in the visible and near-infrared spectrum, Int. J. Heat Mass Transfer 47 (2004) 3643–3648.
[10] J.F. Widmann, J. Duchez, J.C. Yang, J.M. Conny, G.W. Mulholland, Measurement of the optical extinction coefficient of combustion-generated aerosol, Aerosol Sci. 36 (2005) 283–289.
[11] R.A. Dobbins, R.A. Fletcher, H.C. Chang, The evolution of soot precursor particles in a diffusion flame, Combust. Flame 115 (1998) 285–298.
[12] Ü.Ö. Köylü, G.M. Faeth, Optical properties of overfire soot in buoyant turbulent diffusion flames at long residence times, J. Heat Transfer 116 (1994) 152–159.
[13] S.S. Krishnan, K.C. Lin, G.M. Faeth, Extinction and scattering properties of soot emitted from buoyant turbulent diffusion flames, J. Heat Transfer 123 (2001) 331–339.
[14] C.R. Shaddix, A.B. Palotas, C.M. Megaridis, M.Y. Choi, N.Y.C. Yang, Soot graphitic order in laminar diffusion flames and a large-scale JP-8 pool fire, Int. J. Heat Mass Transfer 48 (2005) 3604–3614.
[15] K.A. Jensen, J.M. Suo-Anttila, L.G. Blevins, Characterization of soot properties in two-meter JP-8 pool fires, Sandia National Laboratories Report, SAND2005-0337.
[16] K.C. Smyth, J.E. Harrington, E.L. Johnson, W.M. Pitts, Greatly enhanced soot scattering in flickering CH_4/air diffusion flames, Combust. Flame 95 (1993) 229–239.
[17] C.R. Shaddix, K.C. Smyth, Laser-induced incandescence measurements of soot production in steady and flickering methane, propane, and ethylene diffusion flames, Combust. Flame 107 (1996) 418–452.
[18] J. Zhang, C.M. Megaridis, Soot microstructure in steady and flickering laminar methane/air diffusion flames, Combust. Flame 112 (1998) 473–484.
[19] F.G. Roper, The prediction of laminar jet diffusion flames sizes: Part I. Theoretical model, Combust. Flame 29 (1977) 219–226.
[20] C.R. Shaddix, T.C. Williams, L.G. Blevins, R.W. Schefer, Flame structure of steady and pulsed sooting inverse jet diffusion flames, Proc. Combust. Inst. 30 (2005) 1501–1508.
[21] R.J. Santoro, H.G. Semerjian, R.A. Dobbins, Soot particle measurements in diffusion flames, Combust. Flame 51 (1983) 203–218.
[22] R.J. Santoro, T.T. Yeh, J.J. Horvath, H.G. Semerjian, The transport and growth of soot particles in laminar diffusion flames, Combust. Sci. Technol. 53 (1987) 89–115.
[23] C.M. Megaridis, R.A. Dobbins, The comparison of soot growth and oxidation in smoking and non-smoking ethylene diffusion flames, Combust. Sci. Technol. 66 (1989) 1–16.
[24] R. Puri, T.F. Richardson, R.J. Santoro, R.A. Dobbins, Aerosol dynamics processes of soot aggregates in a laminar ethene diffusion flame, Combust. Flame 92 (1993) 320–333.
[25] R. Puri, The interaction of soot particles with carbon monoxide in laminar diffusion flames, PhD Thesis, Dept. of Mechanical Engineering, Penn State University, Pennsylvania, 1992.
[26] I.M. Kennedy, C. Yam, D.C. Rapp, R.J. Santoro, Modeling and measurements of soot and species in a laminar diffusion flame, Combust. Flame 107 (1996) 368–382.
[27] R.A. Dobbins, C.M. Megaridis, Morphology of flame-generated soot as determined by thermophoretic sampling, Langmuir 3 (1987) 254–259.
[28] R.A. Dobbins, C.M. Megaridis, Absorption and scattering of light by polydisperse aggregates, Appl. Opt. 30 (1991) 4747–4754.
[29] C.M. Sorensen, Light scattering by fractal aggregates: a review, Aerosol Sci. Technol. 35 (2001) 648–687.
[30] S.L. Manzello, M.Y. Choi, Morphology of soot collected in microgravity droplet flames, Int. J. Heat Mass Transfer 45 (2002) 1109–1116.
[31] Ü.Ö. Köylü, Y. Xing, D.E. Rosner, Fractal morphology analysis of combustion-generated aggregates using angular light scattering and electron microscope images, Langmuir 11 (1995) 4848–4854.
[32] W.H. Dalzell, A.F. Sarofim, Optical constants of soot and their application to heat-flux calculations, J. Heat Transfer 91 (1969) 100–104.
[33] K.C. Smyth, C.R. Shaddix, The elusive history of $m = 1.57–0.56i$ for the refractive index of soot, Combust. Flame 107 (1996) 314–320.
[34] S.C. Lee, C.L. Tien, Optical constants of the soot in hydrocarbon flames, Proc. Combust. Inst. 18 (1981) 1159–1166.
[35] J.D. Felske, T.T. Charalampopoulos, H.S. Hura, Determination of the refractive indices of soot particles from the reflectivities of compressed soot pellets, Combust. Sci. Technol. 37 (1984) 263–284.

[36] J. Zhu, M.Y. Choi, G.W. Mulholland, L.A. Gritzo, Soot scattering measurements in the visible and near-infrared spectrum, Proc. Combust. Inst. 28 (2000) 439–446.
[37] G.W. Mulholland, R.D. Mountain, Coupled dipole calculations of extinction coefficient and polarization ratio for smoke agglomerates, Combust. Flame 119 (1999) 56–68.
[38] G.W. Mulholland, C.F. Bohren, K.A. Fuller, Light scattering by agglomerates: coupled electric and magnetic dipole method, Langmuir 10 (1994) 2533–2546.
[39] E. Clar, Polycyclic Hydrocarbons, Academic Press, London and New York, 1964.
[40] R.A. Dobbins, The early soot particle formation in hydrocarbon flames, in: F.L. Dryer, R.F. Sawyer (Eds.), Physical and Chemical Aspects of Combustion: a Tribute to Irvin Glassman, Gordon and Breach Science Publishers, The Netherlands, 1997, pp. 107–133.
[41] P. Minutolo, G. Gambi, A. D'Alessio, The optical band gap model in the interpretation of the UV–visible absorption spectra of rich premixed flames, Proc. Combust. Inst. 26 (1996) 951–957.
[42] R.A. Dobbins, R.A. Fletcher, W. Lu, Laser microprobe analysis of soot precursor particles and carbonaceous soot, Combust. Flame 100 (1995) 301–309.
[43] R.C. Millikan, Sizes, optical properties, and temperatures of soot particles, Temperature: Its Measurement and Control in Science and Industry, vol. 3, Reinhold Publishing, New York, 1962, pp. 497–507.
[44] R. Tsu, J.H. Gonzalez, I.C. Hernandez, Observation of splitting of the E_{2g} mode and two-phonon spectrum in graphites, Solid State Comm. 27 (1978) 507–510.
[45] V.P. Tomaselli, R. Rivera, D.C. Edewaard, K.D. Moller, Infrared optical constants of black powders determined from reflection measurements, Appl. Opt. 20 (1981) 3961–3967.